Atmospheric Environment 309 (2023) 119919

Contents lists available at ScienceDirect

Atmospheric Environment

journal homepage: www.elsevier.com/locate/atmosenv

A signature of aged biogenic compounds detected from airborne VOC measurements in the high arctic atmosphere in March/April 2018

Rupert Holzinger [a,*], Oliver Eppers [b,c], Kouji Adachi [d], Heiko Bozem [b], Markus Hartmann [e,1], Andreas Herber [f], Makoto Koike [g], Dylan B. Millet [h], Nobuhiro Moteki [g], Sho Ohata [g,2,3], Frank Stratmann [e], Atsushi Yoshida [g,4]

[a] Institute for Marine and Atmospheric Research, Utrecht (IMAU), Utrecht University, the Netherlands
[b] Johannes Gutenberg University of Mainz, Institute for Atmospheric Physics, Mainz, Germany
[c] Particle Chemistry Department, Max Planck Institute for Chemistry, Mainz, Germany
[d] Department of Atmosphere, Ocean, and Earth System Modeling Research, Meteorological Research Institute, Tsukuba, Japan
[e] Atmospheric Chemistry Department (ACD), Leibniz-Institute for Tropospheric Research (TROPOS), Leipzig, Germany
[f] Alfred Wegener Institute Helmholtz Centre for Polar and Marine Research (AWI), Bremerhaven, Germany
[g] Department of Earth and Planetary Science, Graduate School of Science, The University of Tokyo, Tokyo, Japan
[h] University of Minnesota, Saint Paul, MN, USA

HIGHLIGHTS

- A PTR-MS instrument onboard the POLAR 5 aircraft detected more than 100 compounds above 1 pmol/mol in at least 25% of the measurements.
- During ozone depletion events enhanced levels of acetone, and methyl-ethylketone, and ice nucleating particles (INP) were observed.
- Acetone and ozone mixing ratios were used as metric for continental influence.
- Continentally influenced air exhibited enhanced signals of biogenic and anthropogenic emissions.
- ~50% of all positively detected compounds (>100) can be associated with terpene oxidation products.

GRAPHICAL ABSTRACT

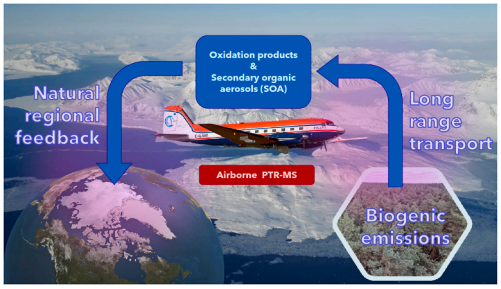

ARTICLE INFO

Keywords:
High arctic
Arctic haze
Biogenic emissions
Ozone depletion events (ODE)

ABSTRACT

During the PAMARCMiP 2018 campaign (March and April 2018) a proton-transfer-reaction mass spectrometer (PTR-MS) was deployed onboard the POLAR 5 research aircraft and sampled the high Arctic atmosphere under Arctic haze conditions. More than 100 compounds exhibited levels above 1 pmol/mol in at least 25% of the measurements. We used acetone mixing ratios, ozone concentrations, and back trajectories to identify periods with and without long-range transport from continental sources. During two flights, surface ozone depletion

* Corresponding author.
E-mail address: r.holzinger@uu.nl (R. Holzinger).
[1] now at: Atmospheric Science, Department of Chemistry and Molecular Biology, University of Gothenburg, Gothenburg, Sweden.
[2] now at: Institute for Space–Earth Environmental Research, Nagoya University, Nagoya, Aichi, Japan.
[3] now at: Institute for Advanced Research, Nagoya University, Nagoya, Aichi, Japan.
[4] now at: National Institute of Polar Research, Tokyo, Japan.

https://doi.org/10.1016/j.atmosenv.2023.119919
Received 19 January 2023; Received in revised form 1 June 2023; Accepted 22 June 2023
Available online 23 June 2023

Proton-transfer-reaction mass-spectrometry (PTR-MS)
POLAR 5

events (ODE) were observed that coincided with enhanced levels of acetone, and methylethylketone, and ice nucleating particles (INP).

Air masses with continental influence contained elevated levels of compounds associated with aged biogenic emissions and anthropogenic pollution (e.g., methanol, peroxyacetylnitrate (PAN), acetone, acetic acid, methylethylketone (MEK), proprionic acid, and pentanone). Almost half of all positively detected compounds (>100) in the high Arctic atmosphere can be associated with terpene oxidation products, likely produced from monoterpenes and sesquiterpenes emitted from boreal forests. We speculate that the transport of biogenic terpene emissions may constitute an important control of the High Arctic aerosol burden. The sum concentration of the detected aerosol forming vapours is ~12 pmol/mol, which is of the same order than measured dimethylsulfide (DMS) mixing ratios and their mass density corresponds to approximately one fifth of the measured non-black-carbon particles.

1. Introduction

The Arctic region is warming more strongly and faster than the rest of the Eart's surface due to complex feedback mechanisms that cause the so-called Arctic amplification (Gulev et al., 2021; Previdi et al., 2021). These feedback loops can be driven by the warming itself or by different types of pollution. Pollution accumulates during the winter in the Arctic region and produces Arctic haze which has the potential to alter cloud properties and thus significantly alter precipitation and the longwave heat balance during the Arctic night. With sunrise in spring the shortwave component adds further complexity. There are no measurements of aerosol and cloud properties during the preindustrial Arctic night making the direct quantification of change an impossible task. However, it is possible to infer the change with good understanding of the undisturbed system. Below we report evidence for a natural process that may have been an important control on High Arctic aerosols before anthropogenic pollution became the dominant control.

In this study we evaluate measurements of atmospheric trace gases in the high Arctic atmosphere during two weeks in March/April 2018 performed onboard the POLAR 5 research aircraft during the PAMARCMiP (Polar Airborne Measurements and Arctic Regional Climate Model simulation Project) campaign (Wesche et al., 2016; Herber et al., 2012). The campaign was conducted after the polar sunrise but still under Arctic haze conditions. This can be seen, for example, in Pernov et al. (2021), who analysed gas phase organics measured at Villum Research Station (VRS)/Station Nord (81.6°N, 16.7°W) in the period April through October 2018, and report an Arctic haze factor that dominated until the end of April but was marginal for the rest of their campaign. The difference between the first few weeks and the rest of their study period is also evident when considering the measured mixing ratios of benzene, an anthropogenic pollutant from fossil fuel and biomass burning. In April Pernov et al. (2021) reported benzene values around 80 pmol/mol, whereas levels stayed below 20 pmol/mol during the summer (June through August). This is strong evidence for two fundamentally different regimes that govern the chemical composition of the High Arctic atmosphere: (i) long-range transport (pollution and natural emissions) and absent local photochemistry during winter (Arctic haze develops with pollution), and (ii) stronger influence from local marine/sea-ice sources and active photochemistry when the polar dome is more isolated and thus long-range import of pollution and natural emissions is reduced. These two regimes also manifest in the regional chemical composition of organic aerosol (OA). Nielsen et al. (2019) report measurements with a soot particle aerosol mass spectrometer covering 93 days in the period Feb–May 2015, at VRS. They found that OA contributed 24% to the total aerosol burden. A positive matrix factorization (PMF) analysis revealed a transition between a component tagged 'Arctic Haze Organic Aerosol' that was active until mid/end April and a 'Marine Organic Aerosol' component that started emerging early in April and dominated OA in May. Considering the 'Arctic haze' factors reported by Pernov et al. (2021), and the timing of the PAMARCMiP campaign, we conclude that the Arctic haze regime dominated during the campaign, but early signs of the transition to the summer regime were likely present as well.

The main goal of this work is identifying possible long-range transport of biogenic emissions to the high Arctic troposphere by exploiting full mass spectra obtained with a PTR-TOF-MS instrument. In several case studies the use of acetone mixing ratios as indicator for continental influence is established. This filter is subsequently applied to the entire dataset and revealed that continentally influenced air not only brings pollution to the High Arctic, but also carries the signature of aged biogenic compounds.

2. Materials and methods

The PAMARCMiP campaign was conducted from Villum Research Station/Station Nord (81.6°N, 16.7°W), Greenland, during March and April 2018. The POLAR 5 research aircraft sampled the Arctic atmosphere during 14 flights that covered a region between 78°N −85°N, 20°W −20°E between 50 and 5000 m above sea level (Herber et al., 2019).

The PTR-MS (PTR-TOF1000, with hexapole ion optics, Ionicon Analytik GmbH, Austria) was mounted aboard the POLAR 5 aircraft and sampled from a shared inlet that consisted of backward facing PFA tubing (length 3 m, ID 9.55 mm) flushed with a constant flow of ~20 L/min. The main airstream was directed to the CO_2/H_2O, CO, and ozone instruments with a ~70 ml/min subflow pulled to the PTR-MS through 2 m of PEEK tubing (ID 1 mm). The PTR-MS drift tube (and inlet system) was heated to 60 °C and operated at a pressure of ~2.8 hPa, and a reduced electric field strength (E/N) of 130 Td. The ion source was supplied with a (gaseous) water flow of 5.5 mL/min (standard conditions, 1013 hPa, 0 °C) that was maintained by a flow controller pulling from the headspace of a reservoir with liquid water. At room temperature, the water saturation vapor pressure is sufficient to maintain the flow, but with cooler temperatures less water vapor is provided to the PTR-MS ion source.

Between flights, all instruments were powerless and the cabin temperature of the POLAR 5 aircraft could be kept above freezing with all available external heating. So, the high vacuum in the PTR-MS could not be maintained between flights, which resulted in relatively high and variable background contamination. Approximately 1 h before take-off the instruments were powered up and cabin temperatures reached ~20 °C during the flight, however, for most flights the water flow into the PTR-MS ion source was not stable during the first hour after take-off. Another issue was encountered at flight levels above ~4200 m when the ambient air pressure became too low to provide sufficient flow into the instrument, which resulted in lower drift tube pressure and higher E/N values. All deviations from standard operation conditions of the PTR-MS reduced the accuracy and quality of the measurements and therefore we focus here on the periods when the instrument performance was at its best –rejecting the first part of all flights and all data collected more than ~4000 m above sea level.

Fig. 1 shows a 1-h segment of acetone measured during flight 2 (March 25, 2018) to illustrate the operation and performance of the instrument. Ambient air was monitored continuously for 180 s while recording data at a frequency of 1 Hz. After every ambient air period a zeroing cycle was performed to determine instrumental noise and

background contamination. Zeroing was done for 20 s (but every 4th time for 40 s, see Fig. 1) by directing the flow through a catalyst that consisted of a 14 cm long stainless steel tube (ID 9 mm), filled with platinum coated quartz wool, and heated to 350 °C. Switching to the catalyst was done with a low internal volume multiport valve (Valco Inc., stainless steel with sulfinert© coating, heated to 60 °C). Volume mixing ratios have been calculated using the PTRwid software (Holzinger, 2015) and the kinetic approach described, for example, by Hansel et al. (1995). The transmission was calibrated by Ionicon Analytik GmbH in December 2017 (together with the installation of the hexapole upgrade) and a gas standard (Apel and Riemer for details see Holzinger et al., 2019) was used to confirm the stability throughout the campaign. For compounds contained in the gas standard we used the reaction rate constants specified in Holzinger et al. (2019), for all other compounds we used a default reaction rate constant of 3×10^{-9} cm^3 s^{-1} $molecule^{-1}$. The instrument featured a sensitivity in the range 400–600 counts per second for mixing ratios at the 1 nmol/mol level, and a mass resolution capacity of 1200 (FWHM). PTRwid processed a unified masslist (Holzinger, 2015) containing 353 ions and for all these ions the signal was extracted and volume mixing ratios were calculated at a 1 s time resolution.

After basic data processing, we produced 10 s averages. This step significantly improved the precision of the data. E.g. we expect a signal of ~20 counts per second from a compound present at 40 pmol/mol in the atmosphere. The relative uncertainty of the data at 1 s time resolution is thus 22% (i.e. sqrt(20)/20) and is reduced to 7% (i.e. sqrt(200)/200) when considering a 10 s time resolution. So, from 180 s of ambient air sampling we formed 18 values and from the zeroing periods we formed 2 or 4 values at 10 s time resolution. In order to subtract instrumental noise and background contamination we calculated a linear fit through the neighbouring 4 or 6 zero measurements and pointwise subtracted the fitted value from the ambient air signal. The linear fit was also used to de-trend the zeroing values that were separated by the 3 min of ambient air sampling. The limit of detection (LOD) was calculated as three times the standard deviation of de-trended 4 or 6 zero measurements. The final dataset contains 7771 values for 353 ions at 10 s time resolution, roughly corresponding to 25 h of measurement.

Supplement Table S1 lists campaign mean volume mixing ratios together with the 25%, 50%, and 75% quantiles for all ions that exhibited signals above the LOD for more than 3% of the 7771 measurements. Supplement Fig. S1 shows the signal detected at 143.109 Th during all flights as an example to illustrate how the 3% threshold has been calculated. All data used in this work are published in a public repository (Holzinger, 2022).

2.1. Auxiliary measurements

A detailed description of the CO and CO_2/H_2O instrument can be found in Bozem et al. (2019). For CO measurements, regular calibrations with a NIST traceable CO standard and zero measurements were used to determine (and correct) for instrument drifts. For PAMARCMiP, the precision of the calculated CO mixing ratio is 1.72 nmol/mol. Similar to CO, calibrations for the CO_2/H_2O instrument were performed in time intervals of 15–30 min using a NIST traceable calibration gas with a known CO_2 mixing ratio and H_2O close to zero. For the campaign, the precision of the instrument is given as 0.04 μmol/mol for CO_2 and 1.7 μmol/mol for H_2O. The temporal stability was calculated from the mean instrumental drift and was estimated with 0.42 μmol/mol for CO_2 and 21.6 μmol/mol for H_2O. Thus, the total uncertainty for CO_2 and H_2O amounts to 0.43 μmol/mol and 22.0 μmol/mol, respectively.

Ozone (O3) mixing ratios were measured using UV absorption at 254 nm with a Dual Beam Ozone Monitor 205 (2B Technologies). UV light passes two separate 15 cm long absorption cells, which are flushed alternately with ozone-filtered and ozone-unfiltered air. The ozone mixing ratios were derived by measuring the absorption ratio as the ratio of the respective intensities for the unfiltered and filtered case. The total uncertainty of the ozone mixing ratios is determined by the instrumental precision and amounts to 1.21 nmol/mol.

Black carbon (BC) and non-absorbing particles (non-BC) in the size range 75–850 nm and 185–850 nm, respectively, were measured by a single-particle soot photometer (SP2; Droplet Measurement Technologies (DMT), Longmont, CO, USA) operated by The University of Tokyo (Yoshida et al., 2020). More information about these measurements can be found in Ohata et al. (2021).

2.2. Back trajectories

The model LAGRANTO (Wernli and Davies, 1997; Sprenger and Wernli, 2015) was used to calculate backward trajectories for the sampled air masses. As meteorological input, operational data from the

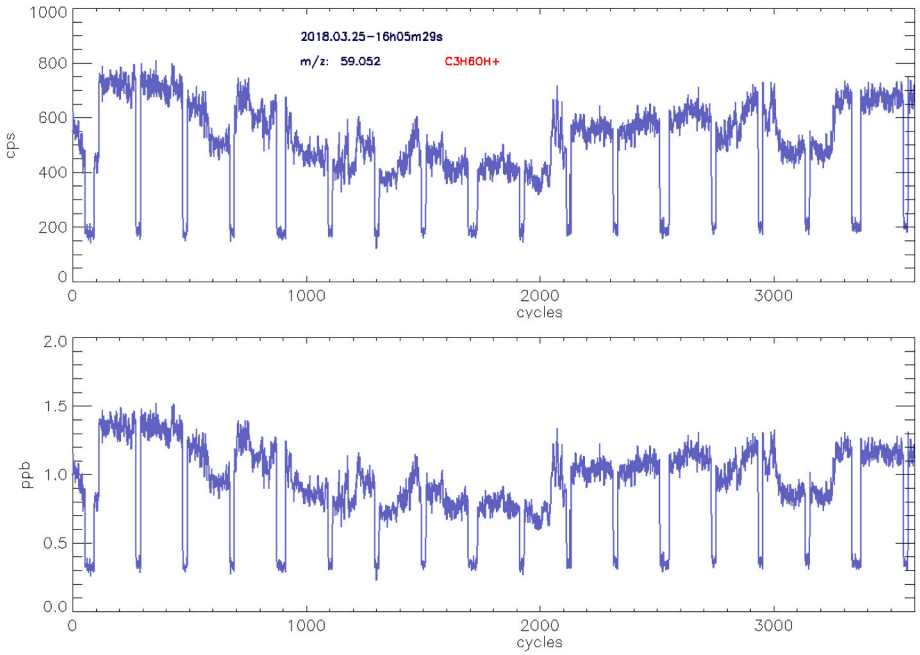

Fig. 1. Output of the PTRwid software (Holzinger, 2015) for the raw signal at 59.052 Th (acetone) during 1 h of flight 2 (March 25, 2018). Three minutes of ambient air sampling are intercepted by periods of zeroing (3 times 20 s, and 40 s every 4th time). Volume mixing ratios are calculated based on simple ion reaction kinetics (Holzinger et al., 2019) using a default reaction rate constant of 3×10^{-9} cm^3 s^{-1} $molecule^{-1}$. The data were recorded at a 1 Hz frequency and the instrument featured a sensitivity around 500 counts per second (cps) for a compound at 1 nmol/mol (ppb).

European Centre for Medium-range Weather Forecast (ECMWF) with 0.125° horizontal resolution and 137 vertical hybrid sigma-pressure levels were used. Trajectories were initialized every 10 s from coordinates along individual research flights and calculated 10 days backward in time. The resolution of the individual output trajectory is 1 h.

3. Results and discussion

3.1. No extensive plumes

Fig. 2 shows flight tracks, and the mixing ratios of acetone and benzene for the 10 flights during which the PTR-MS collected high quality data. A trajectory analysis showed that with a few exceptions the sampled air remained within the Arctic cycle for at least 5 days prior to sampling. Acetone mixing ratios remained in the range 300–1000 pmol/mol and clear variations could be observed. The low acetone mixing ratios suggest that no pollution plumes from biomass burning or other anthropogenic sources have been detected. This idea is supported by stable mixing ratios around 100 pmol/mol of benzene, which is a tracer for all combustion related sources. The observed levels of benzene are typical for Arctic haze conditions and similar levels have been observed at VRS in spring 2018 (Pernov et al., 2021). Fig. 2 reveals that occasionally local plumes from VRS and/or the adjunct military camp Station Nord have been captured towards the end of several flights (see time stamps 31.74, 2.59, and 3.7 in Fig. 2 g,h,i). Toluene is another tracer of combustion sources with similar emission factors as benzene (e.g. Christian et al., 2003; Holzinger et al., 2001). However, the detected mixing ratios of toluene were only ~10 pmol/mol (Supplement Fig. S2), which reflects the five times faster reaction with OH than benzene. The ratio benzene/toluene is typically above 5 which shows that the sampled air was photochemically well aged – aside from the local plumes referenced above. The absence of non-local pollution plumes is in agreement with the low black carbon concentrations that were reported by Ohata et al. (2021) for the same campaign. These authors also report biomass burning plumes; however, these plumes were detected at altitudes above 4500 m and are thus outside the periods evaluated here. Adachi et al. (2021) analysed aerosol filter samples by transmission electron microscopy, and, likewise, they found biomass burning signatures only on filters taken above an altitude of 4000 m.

Acetone mixing ratios exhibit a distinct variation (Fig. 2). The leading assumption is that higher acetone mixing ratios are observed in aged continental air masses that contain biogenic emissions and/or anthropogenic pollution. We will test this hypothesis in the following section.

3.2. Identification of air masses with and without recent continental influence

Benzene mixing ratios exhibited the largest variability during the flight of March 25th, 2018 (Flight 2, Fig. 2 b, and top left chart in Fig. S15). The trajectory analysis also reveals an air source region covering northern Europe to east Asia. The top panels of Fig. 3 show 10 day back trajectories and mixing ratios of acetone during flight 2. Three periods for which trajectories are plotted are specified on the top right panel in green, blue, and magenta, respectively. During the period marked in green, the highest acetone mixing ratios were measured. The trajectory analysis of this period shows that the air was lifted seven days before sampling above Scandinavia and moved at ~3000 m altitude across Siberia to the location of sampling. The period marked in blue also exhibits high acetone mixing ratios. The trajectories move beyond 50°N at high altitudes. Most trajectories have ground contact somewhere between Siberia and the Pacific Ocean to the east of Japan and extend beyond 45°N. The period marked and plotted in magenta is a short episode during the 'blue' period where air with much lower acetone mixing ratios (400 pmol/mol) was sampled. These 10-day back trajectories (plotted in magenta in the top left panel) have no ground contact and they do not extend beyond 50°N. These case studies confirm that higher acetone concentrations can be associated with continental influence.

The bottom panels of Fig. 3 present a case study for flight 7, which was a transfer flight from Longyearbyen, Svalbard, to Station Nord, Greenland, on March 28, 2018. During the first part of the flight (marked in green), the acetone mixing ratios were low, around 300 pmol/mol, and then steeply rose to a high plateau around 900 pmol/mol. The trajectory analysis revealed that the low acetone mixing ratios were associated with air that originated from North Siberia at altitudes above 4000 m. About 7 days prior to sampling the air descended to the surface above the North Atlantic Ocean (westwards of Svalbard). The Greenland ice sheet forced the air upwards and northwards to an altitude of

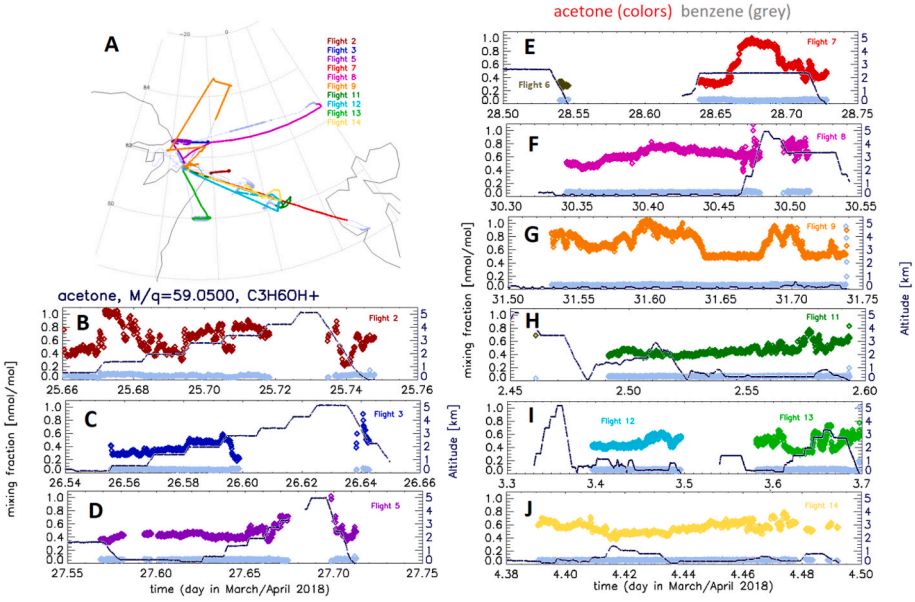

Fig. 2. Flight paths color-coded by the flight number during all periods that are selected for the analysis (a). Panels b–j show acetone and benzene mixing ratios and altitude above sea level for all flights.

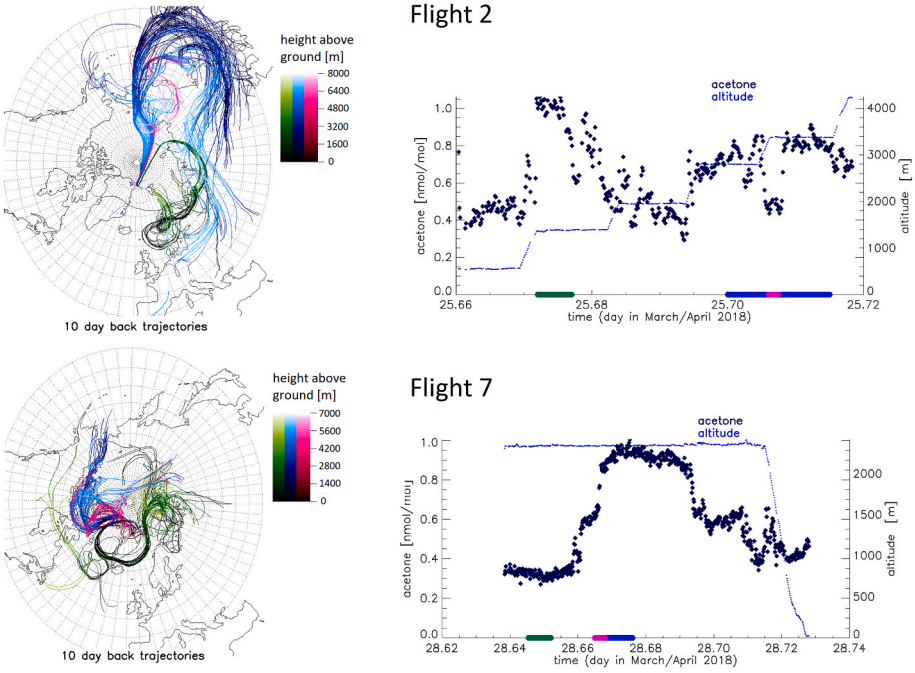

Fig. 3. Case studies during flight 2 (top panels) and flight 7 (bottom panels). The left/right hand panels show back trajectories and mixing ratios of acetone, respectively. The top left panel shows 10-day back trajectories for the periods marked by green, blue, and magenta bars on the x-axis of the top right panel. The trajectories are plotted in a 'fading' colour scale that corresponds to the altitude above ground. The trajectories corresponding to the green bar in the top right panel start exhibit ground contact above Scandinavia approximately 7 days prior to sampling. Flight 7 was a transfer flight from Longyearbyen, Svalbard, to Station Nord, Greenland. The trajectories marked by the green bar in the bottom right panel correspond to the cluster that moves at low altitudes across the North Atlantic and Greenland. See main text for further interpretation.

~2500–3000 m above sea level, followed by an eastward deflection at the same altitude towards the sampling location.

Back-trajectories for the elevated acetone period (marked in blue in the right hand bottom panel of Fig. 3) show that these air masses originate Bering Sea region at altitudes below 1500 m, where they could have picked up continental emissions from West-Alaska and the most Eastern parts of Russia. The continental influence is not as clear from the trajectory analysis as in the previous examples, however, other measured VOCs provide further evidence for the continental influence. For example, enhanced levels of methanol, PAN, MEK, and pentanone

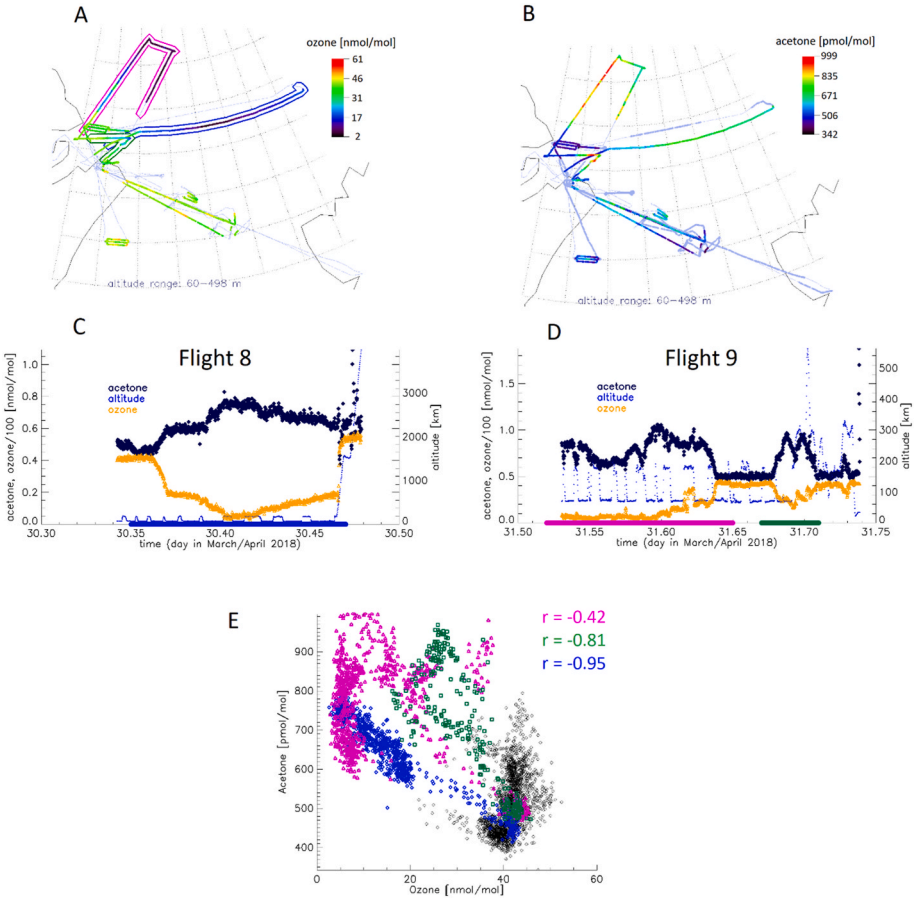

Fig. 4. The top panels show maps with flight tracks and in a colour code the mixing ratios of ozone (a) and acetone (b) for measurements below 500 m. The periods encircled by a blue, magenta, and green line in (a) identify 3 periods during which the ozone levels drop below 20 nmol/mol (encountered during Flights 8 and 9). Ozone and acetone mixing ratios together with flight altitudes during Flights 8 and 9 are shown in (c) and (d), respectively. The marked periods are identified with bars of the same colour at the x-axis. Panel (e) shows a scatter plot of ozone and acetone mixing ratios of these 3 periods (colours) and all remaining data below 500 m altitude.

(Figs. S3, S6, S13, and S17, respectively) clearly show the continental signature, while low levels of acetonitrile (Fig. S4) rule out biomass burning as a source of enhanced VOC concentrations. These case studies show that high acetone levels can be associated with continental influence, however, the ozone depletion events (ODE) discussed in the next section also produce high levels of acetone that are unrelated to continental influence.

3.3. Acetone emissions during ozone depletion events (ODE)

The case studies presented in Fig. 4 show periods of high acetone mixing ratios that cannot be related to continental influence but are linked with emissions from sea ice. The top panels of Fig. 4 show maps with all flight tracks and in a colour code the mixing fractions of ozone (Fig. 4a) and acetone (Fig. 4b) for altitudes below 500 m. In Fig. 4a we see that typical ozone levels in the high Arctic boundary layer were in the range 30–50 nmol/mol, which corresponds to tropospheric background levels in the Northern hemisphere. However, we also identify 3 periods during which the ozone levels drop below 20 nmol/mol. Note that except from these three periods in the planetary boundary layer the ozone mixing ratios were above 30 nmol/mol during all flights. These low-ozone periods (encountered during Flights 8 and 9) are encircled by a blue, magenta, and green line in Fig. 4a. Fig. 4 c and d show ozone and acetone mixing fractions together with flight altitudes during Flights 8 and 9, respectively. The marked periods are identified with bars of the same colour at the x-axis. Fig. 4e is a scatter plot of ozone and acetone mixing ratios of these 3 periods (colours) and all remaining data below 500 m altitude in black. Flights 8 and 9 were dedicated to measurements of sea ice thickness and included very low flight legs at 60 m above the surface that intercepted with slightly higher legs at 180 m above the surface. The low ozone concentrations (Fig. 4a) reveal that ozone depletion events (ODE) were active during these two flights. These events, first reported by Oltmans (1981), have been associated with bromine emission from freshly formed sea ice (see Simpson et al., 2007 and references therein). During flight 8, an inverse relation between ozone and acetone is obvious ($r^2 = 0.91$, blue points in Fig. 4e). The ODE was very shallow during the first part of flight 9 (before 31.55), where acetone was observed to decrease by ~200 pmol/mol whenever the aircraft climbed from 60 m to 180 m. These correlations clearly confirm the emission/production of acetone during ODEs. Yokouchi et al. (1994) reported an inverse correlation between ozone and acetone during ODEs, and Guimbaud et al. (2002) suggested acetone production in the snowpack because the gas phase photooxidation of propane is insufficient to explain the observed levels. Halogen chemistry in snow has been linked to the production of oxygenated VOCs in a couple of previous studies (Sumner et al., 2002; Grannas et al., 2002; Dassau et al., 2004; Simpson et al., 2015; Hornbrook et al., 2016) and fast oxidation pathways have been established with products such as formaldehyde, acetaldehyde, acetone, methylethylketone (MEK), and peroxyacetylnitrate (PAN), but the balance between production and loss is often fragile. For example, Hornbrook et al. (2016) observed enhancement in acetone, MEK, and pentanone, while aldehydes such as formaldehyde and acetaldehyde were depleted during ODEs. Our measurements confirm the emission/production of MEK and pentanone (see Figs. S13 and S17, respectively) during ODEs, exhibiting enhancements that were approximately 35% and 3% of the acetone enhancement, respectively, on a molar basis. For formaldehyde, acetaldehyde and PAN we were not able to detect production or destruction during ODEs, which was due to technical reasons for the aldehydes (poor sensitivity due to high background contamination around the mass to charge ratios of 31 and 45 Th, respectively). Dassau et al. (2004) analysed PAN measurements during ODEs in Alert, Canada, and suggest that PAN production due to fast radical chemistry in the gas phase is balanced by snow pack deposition. So, the PAN mixing ratios may have been stable due to the balance between loss and production during the ODE observed here.

It is worthwhile pointing out that Hartmann et al. (2020) detected enhanced concentrations of ice nucleating particles (INP) that are ice-active at high temperatures during three flights of the PAMARCMIP campaign. With onset temperatures as high as 265.65 K, these enhancements were most pronounced during the two flights with the observed ODE events discussed here. The third flight described in Hartmann et al. (2020) with INP enhancement (onset temperature below 263 K) was flight 2 (discussed above) where back trajectories suggest continental influence from Scandinavia, Siberia, and east Asia. Si et al. (2019) report INP concentrations in the Canadian High Arctic during spring at onset temperatures of 248.15, 253.15, and 258.15 K, respectively. They found that only the 248.15 K INP were correlated with mineral dust – which is known for its capacity to facilitate ice nucleation. Therefore we assume that other types of INP were collected on the filters during the PAMARCMiP campaign, and consequently Hartmann et al. (2020) hypothesize about a local biological process as a source for the observed INP. We hypothesize that such a biogenic source could be linked to the same processes that caused the observed ODE. A biogenic contribution to the bromine emission during ODE events has been suggested for a long time (Barrie et al., 1988; Sturges et al., 1992), so in that respect the co-emission of biological INPs seems plausible. Huang et al. (2021) provide an overview of biological ice nucleating particles in the atmosphere. They highlight the ice nucleating capacity of biological macromolecules (>20 kDa). These structures typically possess areas with very high ice nucleation activity (INA) in the way that hydrophobic and hydrophilic functional groups alternate at distances typical for ice lattice. Condensing water molecules are thus ordered in a way that promotes freezing. Through such a mechanism, biological material can promote ice nucleation at much higher temperatures than other solid surfaces such as mineral dust, so even the high onset temperatures reported by Hartmann et al. (2020) could be understood by this association with the ODE.

3.4. Transport of biogenic compounds to the high Arctic atmosphere

Table 1 shows mean mixing ratios of a number of organic compounds that exhibited mixing ratios above the limit of detection during the periods discussed above. These air masses were classified as continentally influenced (time stamps: 25.67–25.68, 25.70–25.715, 28.67–28.685), Arctic/marine (time stamps: 28.64–28.65, 30.34–30.355, 31.64–31.675, 31.71–31.72), and sea ice/ODE (time stamps: 30.375–30.46 except 30.4–30.42, 30.4–30.42, 31.53–31.625). Figs. S2–S17 include measured mixing ratios during all flights for the compounds shown in Table 1.

Table 1
Mean mixing ratios of compounds during different periods classified as 'continental', 'Arctic/marine', and 'sea ice/ODE'. ***Bold, cursive numbers*** are significantly different from the other two groups (95% confidence).

Detected M/q	**Possible attributions**	Mean mixing ratio ±standard deviation in pmol/mol		
		Continenta	Arctic/marine	Sea ice/ODE
33.021	methanol	***426 ± 92***	152 ± 33	153 ± 38
43.011	$C_2H_3O^+$	***95 ± 36***	34 ± 5.4	36 ± 5.1
45.987	NO_2^+, mostly PAN	***187 ± 78***	70 ± 6.9	61 ± 10
47.013	formic acid	64 ± 38	35 ± 17	23 ± 4.8
57.065	$C_4H_9^+$	36 ± 7.4	32 ± 5.7	33 ± 5.0
59.050	acetone	887 ± 124	***453 ± 88***	733 ± 69
61.030	acetic acid	***57 ± 24***	16 ± 3.4	18 ± 5.9
63.009	DMS	13 ± 2.9	14 ± 7.0	9 ± 1.5
69.069	isoprene	***17 ± 2.8***	12 ± 2.6	10 ± 2.0
73.062	MEK	174 ± 39	***96 ± 18***	172 ± 15
75.043	propionic acid	***17 ± 6.3***	9 ± 2.0	9 ± 0.7
79.055	benzene	66 ± 19	61 ± 2.7	60 ± 3.1
83.081	$C_6H_{11}^+$, cis-3-hexen-1-ol	***12 ± 2.0***	6 ± 2.7	4 ± 1.3
87.055	pentanone	24 ± 7.7	***15 ± 2.0***	23 ± 3.0
93.070	toluene	11 ± 4.3	9 ± 2.0	7 ± 1.1

The levels of benzene and toluene are statistically not different between the three classifications (95% confidence level, 1-tailed student t-test, homoscedastic distribution), reflecting similar levels of (aged) anthropogenic pollution in all air masses. Formic acid, DMS, and $C_4H_9^+$ are also compounds that do not exhibit significant difference. The latter ($C_4H_9^+$) can be associated with anthropogenic hydrocarbon pollution, while high background concentrations and the resulting noise is the likely reason that possible differences could not be resolved for formic acid and DMS. Note that the average mixing ratio of formic acid is still two times higher in continentally influenced air, which is in agreement with Stavrakou et al. (2012) who report satellite evidence for a large source of formic acid from boreal forests. All other compounds listed in Table 1 exhibit significantly higher concentrations in air masses with continental influence compared to air classified as 'Arctic/marine'.

Methanol, acetone, acetic acid, isoprene, MEK, propionic acid, and pentanone can be associated with primary and secondary biogenic emissions (e.g. Oderbolz et al., 2013; Lee et al., 2021), but carbonyls are also produced from photochemical degradation of anthropogenic hydrocarbon pollution. PAN is a stable reservoir of reactive nitrogen that is produced from primary NO_x emissions. $C_2H_3O^+$ is a known fragmentation product in the PTR-MS that is produced from acetic acid with a yield of ~30%. However, the observed levels are about twice as high as the observed signal at 61.03 Th (acetic acid), which suggests that most of this signal must be attributed to other compounds. Possible candidates include thioacetic acid, pyruvic acid, and alkyl acetates (Pagonis et al., 2019), but there are likely additional compounds that produce this ion. $C_6H_{11}^+$ can be tentatively attributed to cis-3-hexen-1-ol, which is a leaf alcohol that has been associated with leaf wounding (Fall et al., 1999). Based on all these case studies we conclude that acetone can be used as a tracer for continental influenced when measurements impacted by ODEs (i.e. ozone below 30 nmol/mol) are removed.

In Fig. 5a-p we show average and median concentrations of anthropogenic (a-h) and biogenic (i-p) components categorized in bins of increasing acetone mixing ratios. Note that for this analysis we removed periods during which ozone was below 30 nmol/mol to avoid any bias from ODE events. All components exhibit the highest mixing ratios in either of the two bins with the highest acetone concentrations. For most components both, average and median, concentrations in these

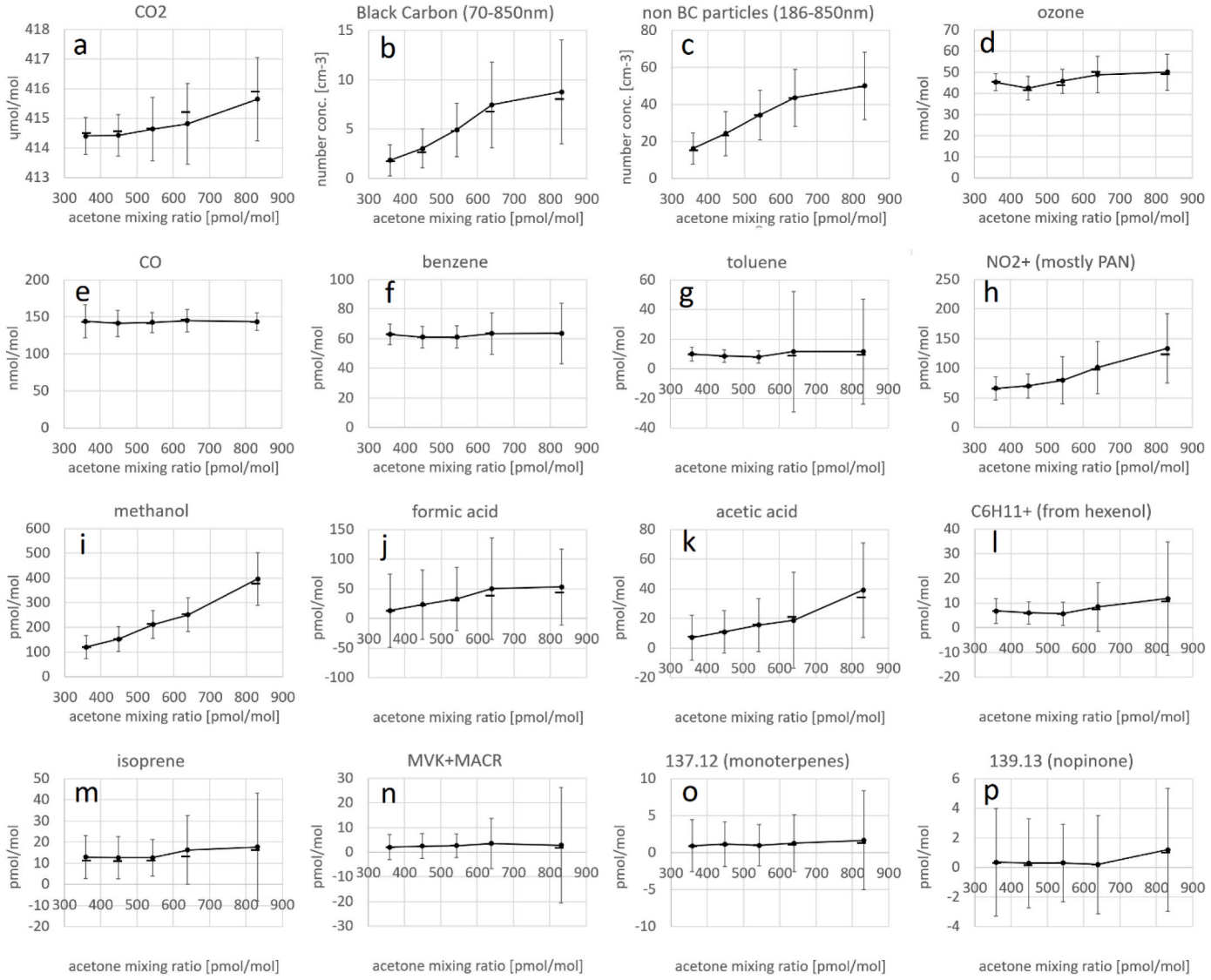

Fig. 5. Average (connected circles) and median (horizontal bars) concentrations of anthropogenic and biogenic components categorized in bins of increasing acetone mixing ratios: 300–400 (n = 1109), 400–500 (n = 2284), 500–600 (n = 1503), 600–700 (n = 613), 700–1000 (n = 590) pmol/mol, respectively. Data exhibiting ozone levels below 30 nmol/mol have been removed from this analysis to avoid biases from ODE events. The error bars represent the standard deviation of all data within a bin. Note that the standard deviation is dominated by statistical noise for mixing ratios below 10 pmol/mol. This figure is reproduced as Supplemental Fig. S18, but without the standard deviation.

two bins are higher than in the three bins with acetone levels below 600 pmol/mol. Anthropogenic pollutants such as CO_2, particles, black carbon, ozone, PAN are enhanced under conditions of high acetone levels. The enhancement is less clear for relative stable pollutants such as CO and benzene, likely due their accumulation during winter Arctic haze. Predominately biogenic compounds such as methanol, formic acid, acetic acid, and the $C_6H_{11}^+$ fragment from cis-3-hexen-1-ol are enhanced as well. Isoprene and its oxidation product MVK + MACR also exhibit an increase with higher acetone levels, however, less pronounced which is likely due to their shorter lifetime. It is remarkable that the signal measured at 137.1 Th (attributed to monoterpenes) and 139.1 Th (attributed to nopinone - a ozonolysis product of β-pinene) are enhanced as well. Considering an ozone concentration of 30 nmol/mol, transport at 253 K and 800 hPa, β-pinene, 3-carene, and α-pinene are the most stable monoterpenes with a lifetime of ~1.6, 0.6, and 0.3 days, respectively (Khamaganov and Hites, 2001). Assuming that the 0.2 pmol/mol increase of median monoterpene mixing ratios (shown in Fig. S18-o) is due to β-pinene, and considering a transport time of 7 days, the mixing ratio at the region of origin should be ~16 pmol/mol, which is consistent with winter mean concentrations above boreal forests reported for the years 2000–2007 (Hakola et al., 2009). On the other hand, for the year 2016 wintertime β-pinene concentrations were reported lower (~1 pmol/mol) at the same site (Hellén et al., 2018). In conclusion, we have to state that the mean and median concentrations for the short lived biogenic compounds in Fig. 5 m-p are at the edge of the detectable range for our instrument, which sets limits to the analysis that we can provide here. However, we note that Fu et al. (2009) quantified several oxidation products from monoterpenes and sesquiterpenes in weekly high-volume aerosol samples from Alert (Canada, 82.5° N, 62.3° W) in the period February to June 1991. Especially during winter and spring, they quantified several oxidation products from monoterpenes and sesquiterpenes, while the samples from June were dominated by isoprene oxidation products.

The data presented in Table 1 and in Fig. 5 show that relatively stable biogenic emissions are transported to the high Arctic, and that the same should be true for isoprene, monoterpenes, and their oxidation products. Emission and photochemical degradation of terpenes (i.e. monoterpenes and sesquiterpenes) are very important for the production of organic aerosol. In order to further explore whether terpene oxidation products are present in the high Arctic atmosphere we exploit a study from Lee et al. (2006). These authors inventoried 73 ions measured by PTR-MS that can be associated with the photooxidation of 11 monoterpenes, 4 sesquiterpenes, and isoprene. Fig. 6 shows the fraction of measurements (n = 7771) above the LOD for all detected ions above 40 Th (n = 318). 66% of the ions thus associated with terpene oxidation products were above the LOD for more than 3% of the measurements. In contrast, only 23% of all other ions were detected above the LOD for more than 3% of the measurements. Of the 104 ions that complied with the latter criterion almost half (48 or 46%) can be associated with terpene oxidation products. This comparison may be an indication of biogenic terpenes and their oxidation products influencing in the high Arctic atmosphere, however, more research is certainly needed to quantify and assess its impact.

Table 2 reproduces the information given in Fig. 6 for the 73 ions identified by Lee et al. (2006) and gives the mean concentration that we measured during the entire campaign (~25 flight hours). To assess the SOA formation potential of these compounds in the high Arctic we consider only compounds heavier than protonated monoterpenes, because these heavier oxidation products efficiently condense on particles. Summing up all compounds heavier than 138.5 Th we estimate that, in average, the Arctic atmosphere contained ~12 pmol/mol of biogenic oxidation products that are expected to partition efficiently into the condensed phase. Considering the limitations of the inlet system and the zeroing method, we think that this is rather a lower limit and that the real content of condensable organics could be larger. Note that the sum mixing ratio of these presumed oxidation products is similar to

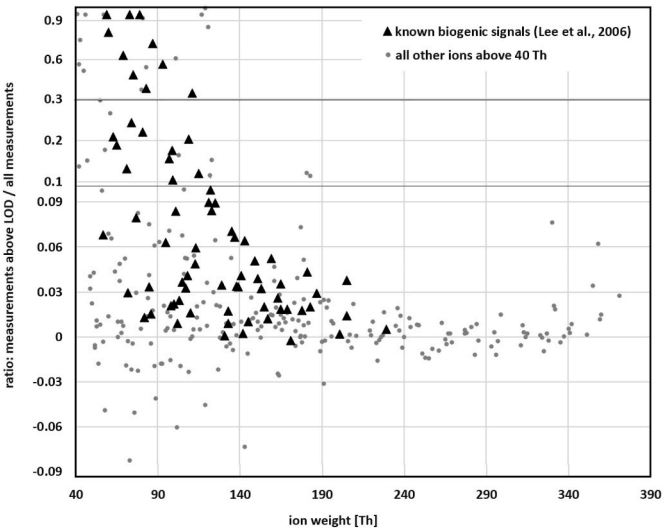

Fig. 6. Fraction of measurements above the limit of detection for all 318 compounds above 40 Th. Terpene oxidation products from Lee et al. (2006) are plotted in black triangles. Negative values indicate compounds that exhibited higher concentrations during the zeroing cycle (contamination). Compounds without clear signal in ambient air are scattered around the zero line.

the measured levels of DMS (see Table 1), and that the mass density of these compounds is typically 20% of the mass of non-BC particles measured during the campaign (size range 185–850 nm, typical volume 0.4 μm^3 cm^{-3}). Both these numbers show that transported terpene oxidation products have the potential to be a key player in controlling the high Arctic aerosol burden during winter. The photochemical degradation of plant volatiles provides material that can be converted to organic aerosol, which may serve as cloud condensation nuclei (CCN). In this way, the vegetation could influence the complex system of aerosol, clouds and radiation in the Arctic region, however, the importance of these processes are not clear and warrant future research that should focus on two main questions: Firstly, could biogenic SOA have been an important factor controlling aerosol/cloud/radiation interaction in the Arctic winter before aerosols from pollution took this role? Secondly, how will climate change influence the import of biogenic emissions to the high Arctic in the future?

4. Summary and conclusions

We analysed a dataset containing 7771 mass spectra (containing 353 ions), each averaged over 10 s, that were obtained with a PTR-MS during 10 flights with the POLAR 5 research aircraft in the high Arctic covering a region between 50 and 4000 m above sea level, and 78°N −85°N, 20°W −20°E. The analysis was aided by back trajectory calculations, and measurements of CO, CO_2, H_2O, ozone, and particles. We were able to show that continentally influenced air contained significantly enhanced levels of aged biogenic and anthropogenic emissions (e.g. methanol, PAN, acetone acetic acid, MEK, proprionic acid, and pentanone) when compared to periods that were classified as Arctic/marine.

During two flights, we encountered ODEs above the sea ice. These events were associated with enhanced acetone, MEK and pentanone mixing ratios, in accordance with findings by Yokouchi et al. (1994), Guimbaud et al. (2002), and Hornbrook et al. (2016). During the same two flights, Hartmann et al. (2020) observed largely enhanced INP concentrations with onset temperatures as high as 265.65 K, which points towards biological INP, i.e. macromolecules that promote freezing of condensing water at high temperatures. The co-occurrence with the ODEs suggests that these biological INP might be emitted along with bromine that causes the ODEs.

An analysis of the full mass spectrum revealed that almost half of the

Table 2
Mean mixing ratio and fraction above the limit of detection for all 73 mass to charge ratios (m/Q) at which Lee et al. (2006) detected terpene oxidation products. Values below 3% are plotted in grey.

m/Q [Th]	mean, pmol/mol	above LOD	m/Q [Th]	mean, pmol/mol	above LOD	m/Q [Th]	mean, pmol/mol	above LOD
57.023	4.9	7%	**100.041**	**0.3**	**2%**	**141.085**	0.6	4%
59.05	561	95%	**101.033**	2.7	8%	**142.028**	**0.0**	**0%**
60.049	18	81%	**102.036**	**0.0**	**1%**	**143.109**	1.2	6%
63.009	9.6	21%	**103.039**	**0.2**	**2%**	**145.066**	**0.3**	**1%**
65.019	3.2	19%	**105.049**	1.0	4%	**149.054**	1.8	5%
69.069	15	63%	**107.047**	2.4	3%	**151.131**	0.6	4%
71.053	4.5	13%	**108.072**	1.9	4%	**153.098**	0.4	3%
72.046	0.6	3%	**109.089**	4.8	20%	**155.115**	**0.3**	**2%**
73.062	118	95%	**110.094**	**0.4**	**2%**	**157.125**	**0.4**	**1%**
74.033	4.3	24%	**111.113**	5.6	34%	**159.093**	1.0	5%
75.043	9.2	49%	**113.041**	0.9	5%	**163.141**	1.9	3%
77.023	1.2	8%	**113.112**	1.1	6%	**165.085**	**0.2**	**2%**
79.055	63	95%	**115.05**	2.6	12%	**165.157**	0.6	4%
81.062	3.8	22%	**121.065**	4.7	9%	**169.061**	**0.2**	**2%**
82.057	0.2	1%	**122.091**	1.4	10%	**171.091**	**−0.2**	**0%**
83.081	7.9	38%	**123.097**	1.4	8%	**178.093**	**0.2**	**2%**
85.056	1.5	3%	**125.119**	1.7	9%	**181.079**	0.5	4%
86.059	**0.1**	**2%**	**129.087**	0.7	3%	**183.089**	0.3	2%
87.055	16	72%	**131.05**	**0.3**	**0%**	**187.084**	0.3	3%
93.07	10	56%	**133.022**	**0.0**	**1%**	**201.097**	**0.0**	**0%**
95.044	2.2	6%	**133.067**	**0.8**	**2%**	**205.101**	**0.2**	**1%**
97.094	3.8	16%	**135.084**	3.2	7%	**205.184**	0.4	4%
98.1	**0.2**	**2%**	**137.123**	1.4	7%	**229.191**	**0.1**	**1%**
99.019	3.6	18%	**138.119**	0.2	3%			
99.076	2.1	10%	**139.129**	0.6	3%			

ions that were above the LOD in at least 3% of the measurements can be associated with oxidation products of terpenes. The presence of terpene oxidation products constitutes a link to organic aerosols because these are well known aerosol precursors. Altogether, our results suggest that long-range transport of biogenic emissions in winter and spring provides a natural source of cloud forming aerosol particles in the high Arctic independent of the pollution that is transported to this region as well. The sum concentration of the detected aerosol forming vapours is ~12 pmol/mol, which is of the same order than measured DMS mixing ratios and their mass density corresponds to approximately one fifth of the measured non-BC particles. The transport of aged biogenic compounds (i.e. monoterpenes and sesquiterpenes from boreal forests) constitutes a natural aerosol source that existed also before the industrial revolution and could have been a natural control of the interaction between aerosols, clouds, and longwave radiation during the high Arctic winter.

CRediT authorship contribution statement

Rupert Holzinger: Design of airborne PTR-MS setup, data processing, Writing – original draft, preparation, Visualization. **Oliver Eppers:** Operation of PTR-MS, ozone, CO2, CO instruments, backtrajectory calculation. **Kouji Adachi:** Particle measurements; all authors proof-read the manuscript and provided input on different aspects of the data analysis, interpretation and presentation. **Heiko Bozem:** all authors proof-read the manuscript and provided input on different aspects of the data analysis, interpretation and presentation. **Markus Hartmann:** all authors proof-read the manuscript and provided input on different aspects of the data analysis, interpretation and presentation. **Andreas Herber:** Flight planning and operation. **Makoto Koike:** Particle measurements; all authors proof-read the manuscript and provided input on different aspects of the data analysis, interpretation and presentation. **Dylan B. Millet:** all authors proof-read the manuscript and provided input on different aspects of the data analysis, interpretation and presentation. **Nobuhiro Moteki:** Particle measurements; all authors proof-read the manuscript and provided input on different aspects of the data analysis, interpretation and presentation. **Sho Ohata:** Particle measurements; all authors proof-read the manuscript and provided input on different aspects of the data analysis, interpretation and presentation. **Frank Stratmann:** all authors proof-read the manuscript and provided input on different aspects of the data analysis, interpretation and presentation. **Atsushi Yoshida:** Particle measurements.

Declaration of competing interest

The authors declare that they have no known competing financial interests or personal relationships that could have appeared to influence the work reported in this paper.

Data availability

Data will be made available on request.

Acknowledgements

Special thanks go to Gernot Hanel and co-workers from Ionicon Analytic GmbH, who assisted during critical trouble shooting after office hours, which was successful despite the poor quality of uncounted satellite voice-only calls connecting North Greenland with Innsbruck, Austria. We gratefully acknowledge the funding by the Deutsche Forschungsgemeinschaft (DFG, German Research Foundation) – project ID 268020496 – TRR 172, within the Transregional Collaborative Research Center "ArctiC Amplification: Climate Relevant Atmospheric and SurfaCe Processes, and Feedback Mechanisms (AC)3".

Appendix A. Supplementary data

Supplementary data to this article can be found online at https://doi.org/10.1016/j.atmosenv.2023.119919.

References

Adachi, K., Oshima, N., Ohata, S., Yoshida, A., Moteki, N., Koike, M., 2018. Compositions and mixing states of aerosol particles by aircraft observations in the Arctic springtime. Atmos. Chem. Phys. 21, 3607–3626. https://doi.org/10.5194/acp-21-3607-2021, 2021.

Barrie, L.A., Bottenheim, J.W., Schnell, R.C., Crutzen, P.J., Rasmussen, R.A., 1988. Ozone destruction and photochemical reactions at polar sunrise in the lower Arctic atmosphere. Nature 334, 138–141.

Bozem, H., Hoor, P., Kunkel, D., Köllner, F., Schneider, J., Herber, A., Schulz, H., Leaitch, W.R., Aliabadi, A.A., Willis, M.D., Burkart, J., Abbatt, J.P.D., 2019.

Characterization of transport regimes and the polar dome during Arctic spring and summer using in situ aircraft measurements. Atmos. Chem. Phys. 19, 15049–15071. https://doi.org/10.5194/acp-19-15049-2019.

Christian, T.J., Kleiss, B., Yokelson, R.J., Holzinger, R., Crutzen, P.J., Hao, W.M., Saharjo, B.H., Ward, D.E., 2003. Comprehensive laboratory measurements of biomass-burning emissions: 1. Emissions from Indonesian, African, and other fuels. J. Geophys. Res. Atmos. 108, 4719. https://doi.org/10.1029/2003JD003704.

Dassau, T.M., Shepson, P.B., Bottenheim, J.W., Ford, K.M., 2004. Peroxyacetyl nitrate photochemistry and interactions with the Arctic surface. J. Geophys. Res. 109, D18302 https://doi.org/10.1029/2004JD004562.

Fall, R., Karl, T., Hansel, A., Jordan, A., Lindinger, W., 1999. Volatile organic compounds emitted after leaf wounding: on-line analysis by proton-transfer-reaction mass spectrometry. J. Geophys. Res. Atmos. 104, 15963–15974.

Fu, P.Q., Kawamura, K., Chen, C., Barrie, L.A., 2009. Isoprene, monoterpene, and sesquiterpene oxidation products in the high arctic aerosols during late winter to early summer. Environ. Sci. Technol. 43, 4022–4028. https://doi.org/10.1021/es803669a.

Grannas, A.M., Shepson, P.B., Guimbaud, C., Sumner, A.L., Albert, M., Simpson, W., Domine, F., Boudries, H., Bottenheim, J., Beine, H.J., Honrath, R., Zhou, X.L., 2002. A study of photochemical and physical processes affecting carbonyl compounds in the Arctic atmospheric boundary layer. Atmos. Environ. 36, 2733–2742. https://doi.org/10.1016/s1352-2310(02)00134-6.

Guimbaud, C., Grannas, A.M., Shepson, P.B., Fuentes, J.D., Boudries, H., Bottenheim, J. W., Domine, F., Houdier, S., Perrier, S., Biesenthal, T.B., Splawn, B.G., 2002. Snowpack processing of acetaldehyde and acetone in the Arctic atmospheric boundary layer. Atmos. Environ. 36, 2743–2752. https://doi.org/10.1016/s1352-2310(02)00107-3.

Gulev, S.K., Thorne, P.W., Ahn, J., Dentener, F.J., Domingues, C.M., Gerland, S., Gong, D., Kaufman, D.S., Nnamchi, H.C., Quaas, J., Rivera, J.A., Sathyendranath, S., Smith, S.L., Trewin, B., von Schuckmann, K., Vose, R.S., 2021. Changing state of the climate system. In: Masson-Delmotte, V., Zhai, P., Pirani, A., Connors, S.L., Péan, C., Berger, S., Caud, N., Chen, Y., Goldfarb, L., Gomis, M.I., Huang, M., Leitzell, K., Lonnoy, E., Matthews, J.B.R., Maycock, T.K., Waterfield, T., Yelekçi, O., Yu, R., Zhou, B. (Eds.), Climate Change 2021: the Physical Science Basis. Contribution of Working Group I to the Sixth Assessment Report of the Intergovernmental Panel on Climate Change. Cambridge University Press, Cambridge, United Kingdom and New York, NY, USA, pp. 287–422. https://doi.org/10.1017/9781009157896.004.

Hansel, A., Jordan, A., Holzinger, R., Prazeller, P., Vogel, W., Lindinger, W., 1995. Proton transfer reaction mass spectrometry: on-line trace gas analysis at the ppb level. Int. J. Mass Spectrom. 149, 609–619. https://doi.org/10.1016/0168-1176(95)04294-U. –150.

Hakola, H., Hellén, H., Tarvainen, V., Bäck, J., Patokoski, J., Rinne, J., 2009. Annual variations of atmospheric VOC concentrations in a boreal forest. Boreal Environ. Res. 14, 722–730.

Hartmann, M., Adachi, K., Eppers, O., Haas, C., Herber, A., Holzinger, R., Hünerbein, A., Jäkel, E., Jentzsch, C., van Pinxteren, M., Wex, H., Willmes, S., Stratmann, F., 2020. Wintertime airborne measurements of ice nucleating particles in the high arctic: a hint to a marine, biogenic source for ice nucleating particles. Geophys. Res. Lett. 47, e2020GL087770 https://doi.org/10.1029/2020GL087770.

Hellén, H., Praplan, A.P., Tykkä, T., Ylivinkka, I., Vakkari, V., Bäck, J., Petäjä, T., Kulmala, M., Hakola, H., 2018. Long term measurements of volatile organic compounds highlight the importance of sesquiterpenes for the atmospheric chemistry of a boreal forest. Atmos. Chem. Phys. 18, 13839–13863. https://doi.org/10.5194/acp-18-13839-2018.

Herber, A., Bozem, H., Hendricks, S., Holzinger, R., Jäkel, E., Koike, M., Neuber, R., Petzold, A., Stratmann, F., 2019. Raw Data of POLAR 5 Campaign PAMARCMiP 2018. PANGAEA. https://doi.org/10.1594/PANGAEA.899508.

Herber, A.B., Haas, C., Stone, R.S., Bottenheim, J.W., Liu, P., Li, S.-M., Staebler, R.M., Strapp, J.W., Dethloff, K., 2012. Regular airborne surveys of Arctic sea ice and atmosphere. Eos 93, 41–42. https://doi.org/10.1029/2012EO040001.

Holzinger, R., Jordan, A., Hansel, A., Lindinger, W., 2001. Automobile emissions of acetonitrile: assessment of its contribution to the global source. J. Atmos. Chem. 38, 187–193. https://doi.org/10.1023/a:1006435723375.

Holzinger, R., 2015. PTRwid: a new widget tool for processing PTR-TOF-MS data. Atmos. Meas. Tech. 8, 3903–3922. https://doi.org/10.5194/amt-8-3903-2015.

Holzinger, R., Acton, W.J.F., Bloss, W.J., Breitenlechner, M., Crilley, L.R., Dusanter, S., Gonin, M., Gros, V., Keutsch, F.N., Kiendler-Scharr, A., Kramer, L.J., Krechmer, J.E., Languille, B., Locoge, N., Lopez-Hilfiker, F., Materic, D., Moreno, S., Nemitz, E., Quéléver, L.L.J., Sarda Esteve, R., Sauvage, S., Schallhart, S., Sommariva, R., Tillmann, R., Wedel, S., Worton, D.R., Xu, K., Zaytsev, A., 2019. Validity and limitations of simple reaction kinetics to calculate concentrations of organic compounds from ion counts in PTR-MS. Atmos. Meas. Tech. 12, 6193–6208. https://doi.org/10.5194/amt-12-6193-2019.

Holzinger, 2022. During the review process the data available at surfdrive (link below). In: After Final Acceptance the Data Will Be Transferred to the UU Repository YODA and Publicly Available with a Unique Digital Object Identifier. https://surfdrive.surf.nl/files/index.php/s/4azfwWI2R4XLkYJ.

Hornbrook, R.S., Hills, A.J., Riemer, D.D., Abdelhamid, A., Flocke, F.M., Hall, S.R., Huey, L.G., Knapp, D.J., Liao, J., Mauldin, R.L., Montzka, D.D., Orlando, J.J., Shepson, P.B., Sive, B., Staebler, R.M., Tanner, D.J., Thompson, C.R., Turnipseed, A., Ullmann, K., Weinheimer, A.J., Apel, E.C., 2016. Arctic springtime observations of volatile organic compounds during the OASIS-2009 campaign. J. Geophys. Res. Atmos. 121, 9789–9813. https://doi.org/10.1002/2015jd024360.

Huang, S., Hu, W., Chen, J., Wu, Z., Zhang, D., Fu, P., 2021. Overview of biological ice nucleating particles in the atmosphere. Environ. Int. 146, 106197 https://doi.org/10.1016/j.envint.2020.106197.

Khamaganov, V.G., Hites, R.A., 2001. Rate constants for the gas phase reactions of ozone with isoprene, α- and β-pinene, and limonene as a function of temperature. J. Phys. Chem. A 105, 815–822. https://doi.org/10.1021/jp002730z.

Lee, A., Goldstein, A.H., Kroll, J.H., Ng, N.L., Varutbangkul, V., Flagan, R.C., Seinfeld, J. H., 2006. Gas-phase products and secondary aerosol yields from the photooxidation of 16 different terpenes. J. Geophys. Res. 111, D17305 https://doi.org/10.1029/2006JD007050.

Lee, X.Q., Huang, D.K., Liu, Q., Liu, X.Y., Zhou, H., Wang, Q., Ma, Y.N., 2021. Underrated primary biogenic origin and lifetime of atmospheric formic and acetic acid. Sci. Rep. 11, 7176. https://doi.org/10.1038/s41598-021-86542-2.

Nielsen, I.E., Skov, H., Massling, A., Eriksson, A.C., Dall'Osto, M., Junninen, H., Sarnela, N., Lange, R., Collier, S., Zhang, Q., Cappa, C.D., Nøjgaard, J.K., 2019. Biogenic and anthropogenic sources of aerosols at the high arctic site Villum research station. Atmos. Chem. Phys. 19, 10239–10256. https://doi.org/10.5194/acp-19-10239-2019.

Ohata, S., Koike, M., Yoshida, A., Moteki, N., Adachi, K., Oshima, N., Matsui, H., Eppers, O., Bozem, H., Zanatta, M., Herber, A.B., 2021. Arctic black carbon during PAMARCMiP 2018 and previous aircraft experiments in spring. Atmos. Chem. Phys. 21, 15861–15881. https://doi.org/10.5194/acp-21-15861-2021.

Oderbolz, D.C., Aksoyoglu, S., Keller, J., Barmpadimos, I., Steinbrecher, R., Skjøth, C.A., Plaß-Dülmer, C., Prévôt, A.S.H., 2013. A comprehensive emission inventory of biogenic volatile organic compounds in Europe: improved seasonality and land-cover. Atmos. Chem. Phys. 13, 1689–1712. https://doi.org/10.5194/acp-13-1689-2013.

Oltmans, S.J., 1981. Surface ozone measurements in clean air. J. Geophys. Res. 86, 1174–1180.

Pagonis, D., Sekimoto, K., de Gouw, J., 2019. A library of proton-transfer reactions of H3O+ ions used for trace gas detection. J. Am. Soc. Mass Spectrom. 30, 1330–1335. https://doi.org/10.1007/s13361-019-02209-3.

Pernov, J.B., Bossi, R., Lebourgeois, T., Nøjgaard, J.K., Holzinger, R., Hjorth, J.L., Skov, H., 2021. Atmospheric VOC measurements at a High Arctic site: characteristics and source apportionment. Atmos. Chem. Phys. 21, 2895–2916. https://doi.org/10.5194/acp-21-2895-2021.

Previdi, M., Smith, K.L., Polvani, L.M., 2021. Arctic amplification of climate change: a review of underlying mechanisms. Environ. Res. Lett. 16, 093003 https://doi.org/10.1088/1748-9326/ac1c29.

Si, M., Evoy, E., Yun, J., Xi, Y., Hanna, S.J., Chivulescu, A., Rawlings, K., Veber, D., Platt, A., Kunkel, D., Hoor, P., Sharma, S., Leaitch, W.R., Bertram, A.K., 2019. Concentrations, composition, and sources of ice-nucleating particles in the Canadian High Arctic during spring 2016. Atmos. Chem. Phys. 19, 3007–3024. https://doi.org/10.5194/acp-19-3007-2019.

Simpson, W.R., von Glasow, R., Riedel, K., Anderson, P., Ariya, P., Bottenheim, J., Burrows, J., Carpenter, L.J., Frieß, U., Goodsite, M.E., Heard, D., Hutterli, M., Jacobi, H.-W., Kaleschke, L., Neff, B., Plane, J., Platt, U., Richter, A., Roscoe, H., Sander, R., Shepson, P., Sodeau, J., Steffen, A., Wagner, T., Wolff, E., 2007. Halogens and their role in polar boundary-layer ozone depletion. Atmos. Chem. Phys. 7, 4375–4418. https://doi.org/10.5194/acp7-4375-2007.

Simpson, W.R., Brown, S.S., Saiz-Lopez, A., Thornton, J.A., Glasow, R., 2015. Tropospheric halogen chemistry: sources, cycling, and impacts. Chem. Rev. 115, 4035–4062. https://doi.org/10.1021/cr5006638.

Sprenger, M., Wernli, H., 2015. The LAGRANTO Lagrangian analysis tool – version 2.0, Geosci. Model Dev. 8, 2569–2586. https://doi.org/10.5194/gmd-8-2569-2015.

Stavrakou, T., Müller, J.-F., Peeters, J., Razavi, A., Clarisse, L., Clerbaux, C., Coheur, P.-F., Hurtmans, D., Mazière, M.D., Vigouroux, C., Deutscher, N.M., Griffith, D.W.T., Jones, N., Paton-Walsh, C., 2012. Satellite evidence for a large source of formic acid from boreal and tropical forests. Nat. Geosci. 5, 26–30. https://doi.org/10.1038/ngeo1354.

Sturges, W.T., Cota, G.F., Buckley, P.T., 1992. Bromoform emission from Arctic ice algae. Nature 358, 660–662. https://doi.org/10.1038/358660a0.

Sumner, A.L., Shepson, P.B., Grannas, A.M., Bottenheim, J.W., Anlauf, K.G., Worthy, D., Schroeder, W.H., Steffen, A., Domine, F., Perrier, S., Houdier, S., 2002. Atmospheric chemistry of formaldehyde in the Arctic troposphere at Polar Sunrise, and the influence of the snowpack. Atmos. Environ. 36, 2553–2562. https://doi.org/10.1016/s1352-2310(02)00105-x.

Wernli, H., Davies, H.C., 1997. A Lagrangian-based analysis of extratropical cyclones. I: the method and some applications. Q. J. Roy. Meteorol. Soc. 123, 467–489. https://doi.org/10.1002/qj.49712353811.

Wesche, C., Steinhage, D., Nixdorf, U., 2016. Polar aircraft POLAR 5 and polar 6 operated by the alfred wegener Institute. J. Large- Scale Res. Facil. 2, A87. https://doi.org/10.17815/jlsrf-2-153.

Yokouchi, Y., Akimoto, H., Barrie, L.A., Bottenheim, J.W., Anlauf, K., Jobson, B.T., 1994. Serial gas-chromatographic mass-spectrometric measurements of some volatile organic-compounds in the arctic atmosphere during the 1992 polar sunrise experiment. J. Geophys. Res. 99 (25 379). –25 389.

Yoshida, A., Moteki, N., Ohata, S., Mori, T., Koike, M., Kondo, Y., Matsui, H., Oshima, N., Takami, A., Kita, K., 2020. Abundances and microphysical properties of light-absorbing iron oxide and black carbon aerosols over East Asia and the Arctic. J. Geophys. Res. Atmos. 125, e2019JD032301 https://doi.org/10.1029/2019JD032301.